Nuclear Instruments and Methods in Physics Research A288 (1990) 649–658
North-Holland

RADID: A SOFTWARE FOR INSERTION DEVICE RADIATION CALCULATION

Chunxi WANG and Dingchang XIAN

Synchrotron Radiation Laboratory BEPC, Institute of High Energy Physics, Academia Sinica, Beijing 100039, P.R. China

Received 19 July 1989

A new software is developed at the Synchrotron Radiation Laboratory BEPC, to calculate radiation distributions from insertion devices of one-dimensional linearly polarized magnetic fields. Based on classical electrodynamics, most factors concerned in such devices are analyzed in detail. According to the radiation mechanism, an efficient calculation method was developed which can be viewed as a natural extension of the bending magnet calculation method. The obtained algorithm has been implemented by VAX Fortran, and resulted in a powerful and easy-to-use software. Using this software, the radiation distribution of insertion devices having arbitrary field distribution can be calculated, with the electron beam emittance effect as well as the finite observation distance effect taken into consideration. Using this software, not only the radiation distribution can be calculated, but also the functions of various factors in the radiation can be analyzed, so it is helpful for a better understanding of the radiation properties. This software can output the calculated results either in numerical data or graphs, and is a powerful tool for designing and building insertion devices and beam lines.

1. Introduction

Insertion devices (IDs) are widely used in synchrotron radiation facilities all over the world to acquire harder X-rays or higher brilliance [1,10]. Most of these devices in use now are magnets providing a linearly polarized magnetic field, which depends only on the axial coordinate of these devices. They can be expressed by (see fig. 1):

$$\boldsymbol{B} = B_{\max} B_y(z)\boldsymbol{e}_y. \tag{1}$$

Usually $B_y(z)$ are periodic (e.g. sin z) for undulators; quasi-periodic for multipole wigglers and strange-formed for wavelength shifters. We shall assume $B_y(z)$ an arbitrary but well-behaved function.

This paper describes a new software developed at the Synchrotron Radiation Laboratory, BEPC, for calculations of the radiation properties of such insertion devices.

Although theoretical analyses are well-known [1,6–8], a numerical method is necessary to calculate the radiation properties accurately, mainly because of the electron beam emittance effect, finite observation distance effect and arbitrary form of the magnetic field $B_y(z)$ [3–5].

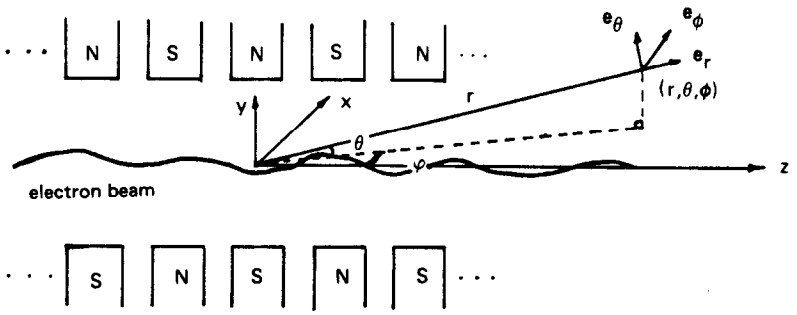

Fig. 1. Orientation of the axes with respect to the insertion device.

0168-9002/90/$03.50

Despite the fact that many programs exist for such calculations, none of them can include all the above mentioned factors, and not one is widely used. Our new software was aimed to take all these factors into consideration and, moreover, much effort was paid to make the software efficient and easy-to-use.

In the following sections, we shall describe the physical basis of our algorithm, outline the main features of our new software and discuss a few results of this software. Throughout this paper, mks units are used.

2. Algorithm and physics

We find that the electron orbits under eq. (1) can be described most adequately for numerical calculation as:

$$
\begin{aligned}
&\beta_x(z) = \beta_x(z_0) + \frac{\kappa}{c}\int_{z_0}^{z} B_y(z)\,\mathrm{d}z;\\
&1-\beta_z = 1-\sqrt{\beta^2-\beta_y^2-\beta_x^2};\\
&\beta_y(z) = \beta_y(z_0);\\
&D_\mathrm{p}(z) \equiv ct - z;\\
&D_\mathrm{p}(z) = D_\mathrm{p}(z_0) + \int_{z_0}^{z}\left(\frac{1}{\beta_z}-1\right)\mathrm{d}z;\\
&x(z) = x(z_0) + \int_{z_0}^{z}\frac{\beta_x}{\beta_z}\mathrm{d}z;\\
&y(z) = y(z_0) - \beta_{y_0}\left[D_\mathrm{p}(z_0)+z_0\right] + \beta_{y_0}\left[D_\mathrm{p}(z)+z\right];\\
&1-\langle\beta_z\rangle_t = \left(1+\frac{\Delta z}{\Delta D_\mathrm{p}}\right)^{-1};
\end{aligned}
\tag{2}
$$

where:

$$
\kappa = \omega_\mathrm{d}\delta;\quad \omega_\mathrm{d} = \frac{2\pi c}{\lambda_\mathrm{d}};\ \delta = \frac{K}{\gamma} = \frac{eB_\mathrm{max}}{\gamma m_\mathrm{e}\omega_\mathrm{d}};\quad K = \frac{eB_\mathrm{max}\lambda_\mathrm{d}}{m_\mathrm{e}2\pi c} = 0.934\,\lambda_\mathrm{d}[\mathrm{cm}]B_\mathrm{max}[\mathrm{T}].
$$

λ_d is the space period of the ID. Deflection parameter K characterizes the nature of the ID, its value ranges from $K \le 1$ for undulators and to $K \gg 1$ for wigglers [12].

According to electrodynamics, the radiation is governed by [2]:

$$
\frac{\mathrm{d}^2 I}{\mathrm{d}\omega\,\mathrm{d}\Omega} = \frac{1}{4\pi\epsilon_0}\frac{e^2}{4\pi^2 c}\left|\int_{-\infty}^{+\infty}\frac{\boldsymbol{n}\times\left[(\boldsymbol{n}-\boldsymbol{\beta})\times\dot{\boldsymbol{\beta}}\right]}{(1-\boldsymbol{n}\cdot\boldsymbol{\beta})^2}\mathrm{e}^{\mathrm{i}\omega(\tau+R(\tau)/c)}\,\mathrm{d}\tau\right|^2. \tag{3}
$$

For most cases, using far field approximation, eq. (3) can be simplified to the following form:

$$
\frac{\mathrm{d}^2 I}{\mathrm{d}\omega\,\mathrm{d}\Omega} = \frac{1}{4\pi\epsilon_0}\frac{e^2\omega^2}{4\pi^2 c}\left|\int_{-\infty}^{+\infty}\boldsymbol{n}\times(\boldsymbol{n}\times\boldsymbol{\beta})\,\mathrm{e}^{\mathrm{i}\omega(\tau-\boldsymbol{n}\cdot\boldsymbol{x}_\mathrm{e}/c)}\,\mathrm{d}\tau\right|^2. \tag{4}
$$

But for some cases, the finite observation distance effect needs to be included for accurate calculations. Following the same consideration in obtaining eq. (4) from eq. (3), we have:

$$
\frac{\boldsymbol{n}\times\left[(\boldsymbol{n}-\boldsymbol{\beta})\times\dot{\boldsymbol{\beta}}\right]}{(1-\boldsymbol{n}\cdot\boldsymbol{\beta})^2} = \frac{\mathrm{d}}{\mathrm{d}t}\frac{\boldsymbol{n}\times(\boldsymbol{n}\times\boldsymbol{\beta})}{1-\boldsymbol{n}\cdot\boldsymbol{\beta}} + \frac{c}{R}\left\{\frac{(\boldsymbol{n}\times\boldsymbol{\beta})^2}{1-\boldsymbol{n}\cdot\boldsymbol{\beta}}\boldsymbol{n} + \frac{\boldsymbol{n}\times(\boldsymbol{n}\times\boldsymbol{\beta})}{1-\boldsymbol{n}\cdot\boldsymbol{\beta}}\left[1-\frac{1}{\gamma^2(1-\boldsymbol{n}\cdot\boldsymbol{\beta})}\right]\right\}. \tag{5}
$$

It can easily be shown that the maximum modification caused by the second term of eq. (5) is:

$$\frac{\gamma c}{R\omega} = \gamma \frac{\lambda}{R} \ll 1, \tag{6}$$

and the maximum modification caused by the third term of eq. (5) is:

$$\frac{2\gamma^2 c}{R\omega} = 2\gamma^2 \frac{\lambda}{R}. \tag{7}$$

So, if the observation distance $r \gg 2\gamma^2\lambda$, eq. (3) can be simplified to

$$\frac{\mathrm{d}^2 I}{\mathrm{d}\omega\, \mathrm{d}\Omega} = \frac{1}{4\pi\epsilon_0} \frac{e^2\omega^2}{4\pi^2 c} \left| \int_{-\infty}^{+\infty} \boldsymbol{n} \times (\boldsymbol{n} \times \boldsymbol{\beta})\, \mathrm{e}^{\mathrm{i}\omega(\tau + R(\tau)/c)}\, \mathrm{d}\tau \right|^2, \tag{8}$$

where $\boldsymbol{n}$ is no longer constant.

To get the phase difference between eqs. (8) and (4), we expand

$$R(\tau) = r - \boldsymbol{n}_o \cdot \boldsymbol{x}_e + \frac{x_e^2}{r - x_e}(1 - \boldsymbol{n}_o \cdot \hat{\boldsymbol{x}}_e) + \cdots, \tag{9}$$

and the phase modification is determined by:

$$\frac{\omega}{2c} \frac{x_e^2}{r - x_e} [\angle(\boldsymbol{n}_o, \hat{\boldsymbol{x}}_e)]^2. \tag{10}$$

The effect of this term can not be neglected in many cases, and was discussed analytically in ref. [6]. In order to be able to include the near field effect, our software is now based on eq. (8) and the influence of eq. (7) can be taken into account easily if necessary.

The main difficulty of calculating eq. (8) comes from the phase factor. It usually oscillates rapidly and makes ordinary numerical integration methods inadequate. Generally, such an oscillation function is integrated approximately by stationary phase or saddle point methods [5].

The phase at arbitrary position can be calculated adequately by:

$$\Phi(z) = \frac{\omega}{c}\left[D_p(z) + (r - z)\epsilon(1 - \epsilon/2)\right] \quad \text{and}$$

$$\epsilon \equiv \left(\frac{r}{r - z_e}\right)^2 \left[\frac{z}{r}(1 - \cos\theta\cos\phi) - \frac{x}{r}\left(\cos\theta\sin\phi - \frac{x}{2r}\right) - \frac{y}{r}\left(\sin\theta - \frac{y}{2r}\right)\right], \tag{11}$$

where r is the distance between the observation point and the chosen origin (e.g. center of ID, see fig. 1).

To simplify eq. (8) we expand the phase as:

$$\Phi(\tau) = \Phi(\tau_0) + \frac{\omega}{\omega_d} \sum_{n=1}^{\infty} \frac{1}{n!} f_n [\omega_d(\tau - \tau_0)]^n, \tag{12}$$

where:

$$\begin{cases} f_1 = 1 - \beta_0 \\ f_2 = -\delta B_y \beta_- + \dfrac{c}{R\omega_d}(\beta^2 - \beta_0^2) \\ f_3 = (\delta B_y)^2 \beta_+ - \delta B_y \dfrac{\dot{B}_y}{\omega_d B_y} \beta_- - 3\dfrac{c}{R\omega_d} \delta B_y \beta_0 \beta_- + 3\left(\dfrac{c}{R\omega_d}\right)^2 (\beta^2 - \beta_0^2)\beta_0 \\ \cdots \end{cases}$$

and

$$\beta_0 \equiv \hat{R}\cdot\boldsymbol{\beta} = \frac{r\cos\theta\cos\phi - z}{R}\beta_z + \frac{r\cos\theta\sin\phi - x}{R}\beta_x + \frac{r\sin\theta - y}{R}\beta_y,$$

$$\beta_+ \equiv \hat{R}\cdot\boldsymbol{\beta}_+ = \frac{r\cos\theta\cos\phi - z}{R}\beta_z + \frac{r\cos\theta\sin\phi - x}{R}\beta_x,$$

$$\beta_- \equiv \hat{R}\cdot\boldsymbol{\beta}_- = \frac{r\cos\theta\cos\phi - z}{R}\beta_z - \frac{r\cos\theta\sin\phi - x}{R}\beta_x.$$

It was found that at positions satisfying $\hat{R}\parallel\boldsymbol{\beta}$, the phase has the following good properties:

1. First-order term is minimum and is almost zero.
2. Second-order term vanishes, which means the above property is stable.
3. The expanded expression is easy to calculate.
4. The resulted method can be viewed as a natural extension of bending magnet calculation method, and is in the spirit of the stationary phase method.

So, the condition $\hat{R}\parallel\boldsymbol{\beta}$ is good for the choice of expanding points. But it is too strong for practical use, and we instead adapt a slightly weaker condition as:

$$\hat{R}\cdot\dot{\boldsymbol{\beta}} = 0, \tag{13}$$

which means the projection of $\hat{R}$ on the orbit plane is parallel to $\boldsymbol{\beta}$.

In order to obtain the expansion points, eq. (13) can be written as:

$$\phi \simeq \tan\phi \simeq \frac{\frac{x}{r} + \left(1 - \frac{z}{r}\right)\beta_x}{\frac{z}{r} + \left(1 - \frac{z}{r}\right)\beta_z}, \tag{14}$$

where ϕ is the horizontal observation angle.

Eq. (14) represents a multi-valued function $\phi(z)$, and its inversion gives expansion points $Z(\phi)$ corresponding to observation angle ϕ; then the various orbit values at expansion points can be obtained.

Under the condition of eq. (13), eq. (12) can be reduced to:

$$\Phi(\tau) = \Phi_s + \frac{\omega}{\omega_d}\left[\frac{1}{2\gamma^2} + \frac{1}{2}\left(\frac{r}{R}\theta - \frac{y}{R} - \frac{\beta_y}{\beta}\right)^2\right]\left[\omega_d(\tau - \tau_s)\right] + \frac{1}{6}\frac{\omega}{\omega_d}(\delta B_y)^2\left[\omega_d(\tau - \tau_s)\right]^3 + \cdots, \tag{15}$$

where the zero order term Φ_s can be calculated by eq. (11).

Generally, there is no need to include higher-order terms in this expansion, but when the gradient of the magnetic field is big enough, we may need to include terms such as $\mathrm{d}B_y/\mathrm{d}z$, (mainly the fifth-order terms). For brevity, we will not go into this problem in detail, and retain in our software only up to the third-order terms.

For later use, eq. (15) is transformed into

$$\Phi(\xi) = \Phi_s + \tfrac{3}{2}\zeta\left(\xi + \frac{\xi^3}{3}\right), \tag{16}$$

where:

$$\xi = \sigma_s\omega_d(\tau - \tau_s),$$

$$\sigma_s = \delta\,|B_y|\left[\frac{1}{\gamma^2} + \left(\frac{r}{R}\theta - \frac{y}{R} - \frac{\beta_y}{\beta}\right)^2\right]^{-1/2},$$

$$\zeta = \frac{1}{3}\frac{\omega}{\omega_d}\frac{1}{\delta\,|B_y|}\left[\frac{1}{\gamma^2} + \left(\frac{r}{R}\theta - \frac{y}{R} - \frac{\beta_y}{\beta}\right)^2\right]^{3/2}.$$

In the neighborhood of the expansion point, the vector part of eq. (8) can be expanded as:

$$\begin{aligned} \boldsymbol{n}\times(\boldsymbol{n}\times\boldsymbol{\beta}) &= \boldsymbol{n}\times(\boldsymbol{n}\times\boldsymbol{\beta})\,|_s - \delta\boldsymbol{n}\cdot\boldsymbol{\beta}\boldsymbol{n}\times\boldsymbol{B}_y\omega_d(\tau-\tau_s)+\cdots \\ &= \left(\frac{\beta_{y_0}}{\beta}+\frac{y}{R}-\frac{r}{R}\theta\right)\boldsymbol{e}_\theta - \delta B_y\omega_d(\tau-\tau_s)\boldsymbol{e}_\phi+\cdots. \end{aligned} \tag{17}$$

Combining eqs. (8), (16) and (17) we get:

$$\begin{aligned} \frac{d^2I}{d\omega\,d\Omega} \simeq \frac{1}{4\pi\epsilon_0}\frac{e^2}{4\pi^2c}\left(\frac{\gamma m}{eB_{max}}\omega\right)^2\Bigg\{&\left|\sum_s\left(\frac{r}{R}\theta-\frac{y}{R}-\frac{\beta_y}{\beta}\right)\left(\frac{\delta}{\sigma_s}\right)e^{i\Phi_s}\int_{\Gamma_s}e^{i\frac{1}{2}\zeta(\xi+\xi^3/3)}\,d\xi\right|^2 \\ &+\left|\sum_s B_y\left(\frac{\delta}{\sigma_s}\right)^2 e^{i\Phi_s}\int_{\Gamma_s}\xi\, e^{i\frac{1}{2}\zeta(\xi+\xi^3/3)}\,d\xi\right|^2\Bigg\}, \end{aligned} \tag{18}$$

where Γ_s is an adequate neighborhood of the stationary point s, and Σ_s means the sum over all stationary points.

For wigglers, Γ_s can be replaced by $(-\infty, \infty)$ with sufficient accuracy; then the flux of beam radiation without considering the emittance effect is:

$$\begin{aligned} \frac{d^2F}{d\theta\,d\phi} = \frac{\alpha}{3\pi^2}\frac{I}{e}\frac{\Delta\omega}{\omega}\left(\frac{\gamma m}{eB}\omega\right)^2 \\ \times\left\{\left|\sum_s\left(\frac{r}{R}\theta-\frac{y}{R}-\frac{\beta_y}{\beta}\right)\left(\frac{\delta}{\sigma_s}\right)e^{i\Phi_s}K_{1/3}(\zeta_s)\right|^2+\left|\sum_s B_y\left(\frac{\delta}{\sigma_s}\right)^2 e^{i\Phi_s}K_{2/3}(\zeta_s)\right|^2\right\}, \end{aligned} \tag{19}$$

where α is the fine-structure constant, $K_{1/3}$, $K_{2/3}$ are the modified Bessel functions.

For IDs of high K-value, eq. (19) can be used to calculate the spectra accurately and efficiently, and our software mainly relies on it. For undulators, eq. (18) can be used, and the results may not be very accurate but are still good enough in most cases. Direct numerical integration based on the adaptive Gaussian quadrature method is also provided for.

Many other formula can be deduced from eqs. (18) or (19) by simplifying the summation Σ_s for special cases. For example, incoherent summation can be used for wigglers; summation on the whole range can be reduced to be on just one period for periodic devices, and so on. We will not describe them further.

Eqs. (19) and (18) can be viewed as a natural extension of bending magnet radiation. The important feature of them is the appearance of the term $(r/R)\theta - y/R - \beta_y/\beta$, which reflects the influence of observation distance and beam emittance. From this term, we can directly obtain the well-known modification factor eq. (20) for nonzero emittance, if we assume all variables have a Gaussian distribution.

$$\frac{\sigma_\theta}{\sqrt{\sigma_\theta^2+\left(\frac{\sigma_y}{R}\right)^2+\sigma_{y'}^2}}, \tag{20}$$

where σ_θ is the vertical angle deviation of single particle radiation.

For consideration of the beam emittance effect, we use the Monte Carlo method in the software. The electron beam is simulated by the following distribution [8]:

$$P(x, x') = \frac{1}{2\pi\epsilon_x}e^{-\frac{1}{2\epsilon_x}(\gamma_x x^2+2\alpha_x xx'+\beta_x x'^2)}\,dx\,dx', \tag{21}$$

where:

$$\langle x^2\rangle = \beta_x\epsilon_x;\quad \langle x'^2\rangle = \gamma_x\epsilon_x;\quad \gamma_x = (1+\alpha_x^2)/\beta.$$

ϵ_x is the emittance, β_x is the amplitude function and γ_x, α_x are the Twiss parameters.

Transforming to a standard binary normal distribution, we have:

$$P(x, x') = \frac{1}{2\pi\sigma_x\sigma_{x'}\sqrt{1-\rho^2}} e^{-\frac{1}{2(1-\rho^2)}\left(\frac{x^2}{\sigma_x^2} - 2\rho\frac{xx'}{\sigma_x\sigma_{x'}} + \frac{x'^2}{\sigma_{x'}^2}\right)} dx\, dx', \tag{22}$$

where:

$$\sigma_x = \sqrt{\beta_x\epsilon_x}; \quad \sigma_{x'} = \sqrt{\gamma_x\epsilon_x}; \quad \rho = \sqrt{1-(\epsilon_x/\sigma_x\sigma_{x'})^2}.$$

At the entrance of the ID, the electron beam phase space can be simulated by the standard Monte Carlo method:

$$\begin{aligned} x &= x_0 + \sigma_x\sqrt{-2\ln u}\left(\sqrt{1-\rho^2}\cos 2\pi v + \rho \sin 2\pi v\right), \\ x' &= x_0' + \sigma_{x'}\sqrt{-2\ln u}\sin 2\pi v, \end{aligned} \tag{23}$$

where u, v are random variables uniformly distributed between (0, 1).

Combining the Monte Carlo method and eqs. (19) or (18), we can take into account both the near field effect and the emittance effect.

For practical use, this software includes filter absorption calculations, and the method was borrowed from the widely used software SHADOW [11]. Apertures will be added in the near future.

3. Features of RADID

The above algorithm has been implemented by VAX Fortran on VAX/VMS system, and resulted in a software we called RADID, which stands for RADiation of Insertion Devices. This section will describe its main features, but will not list all its functions.

The most important feature of RADID, as already emphasized above, is the capability of including all important factors such as beam emittance, observation distance, edge field effect or a magnetic field of specific shape, window's absorption, etc., in calculation. Furthermore, one can choose between speed and accuracy, because lots of calculation routines with different accuracy and speed have been implemented for various calculation purposes. Generally speaking, ID radiation calculations are very time-consuming, and the more factors are considered, the more CPU-time is demanded.

For example, a multipole device can be viewed as a one-period device and one can use eq. (19) to calculate, or can be viewed as a multi-period device and one can use eq. (19) to calculate just one period, and then multiply by a coherent factor. The first way may be more accurate than the second one, but certainly is much slower if the period number is big.

Another attractive feature is that RADID can handle almost all properties of ID radiation one is interested in. For example, one can choose photons or powers as output; one can integrate the photon energy and angles over the whole range or over a specified range; one can add any number of windows or filters and output the part of radiation transmitted through or absorbed in the last filter, so it is easy to calculate the absorption in a sample or a detector.

Besides the above features of the main program, many satellite programs such as BEAM and PHASE are provided. These enable one to get information about the electron beam (eqs. (2), (4), etc.)), phase function (eqs. (11), (15), (13), etc.)) and our expansion approximation. So these satellite programs can help one to understand the radiation properties and monitor the validity of various approximations.

In order to make the software easy-to-use, a convenient user interface has been implemented, such as default input mechanism, automatic submit of batch jobs, and so on.

Another very important feature is that it enables graphic output automatically, which is helpful for the understanding of the results and is very efficient for representing radiation properties. The graphics are created with the Top-Drawer graphics package of SLAC.

4. Some results and discussion

As an example of the application of RADID, in the following we give the results of the synchrotron radiation from the wavelength shifter SRW1 at the Synchrotron Radiation Laboratory BEPC. Some other primary usage of RADID was contained in ref. [9].

Fig. 2 is the designed magnetic field $B_y(z)$ with a long segment of uniform field which serves as a bending magnet. The peak field $B_{max} = 1.84$ T.

Fig. 3 represents the magnetic field corresponding to the tangential angle of the beam orbit. This figure shows the number of radiation points with their field strengths for different horizontal observation angles, so it is very helpful for the understanding of the horizontal radiation distribution characteristics. The curve must be closed because a real ID must satisfy the condition $\oint B_y \, dz = 0$. The above two figures are among the outputs of the satellite program BEAM.

Fig. 4 shows the phase eq. (11) at a photon energy of 1 keV. Pay attention to the rapid change of the phase. Our expansion eq. (15) and stationary point eq. (13) are plotted out also. This is a typical output of another satellite program PHASE. It is helpful to understand our algorithm and radiation properties. Moreover, it can serve as a monitor of the phase expansion approximation in use.

The following figs. demonstrate the calculated radiation distributions of the above mentioned wavelength shifter. The near field and beam emittance effects are shown. In the near field case, 10 m is used. When emittance is concerned, the number of Monte Carlo sample points used is 1000 and the beam

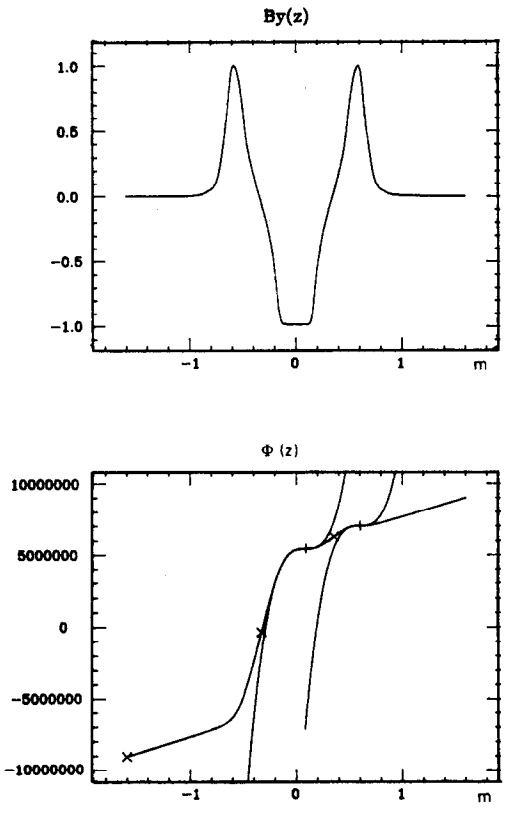

Fig. 2. The designed magnetic field $B_y(z)$.

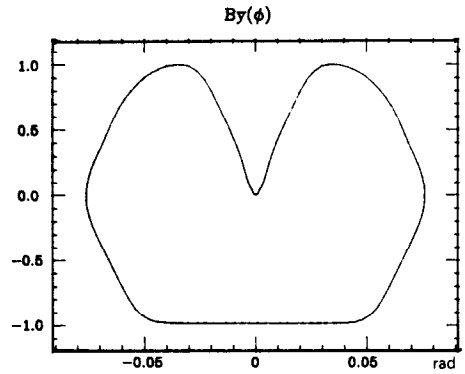

Fig. 3. The magnetic field vs the tangential angle of the beam orbit.

Fig. 4. The phase and expansion used.

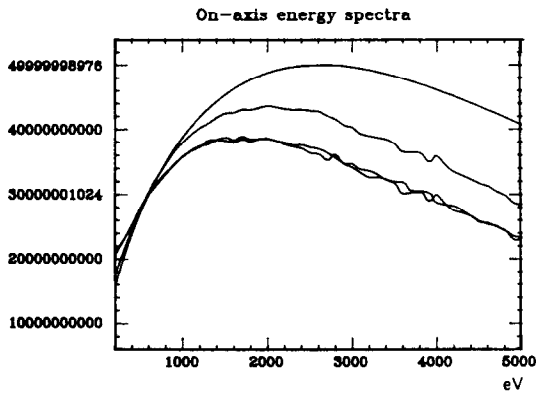

Fig. 5. The on-axis flux spectrum.

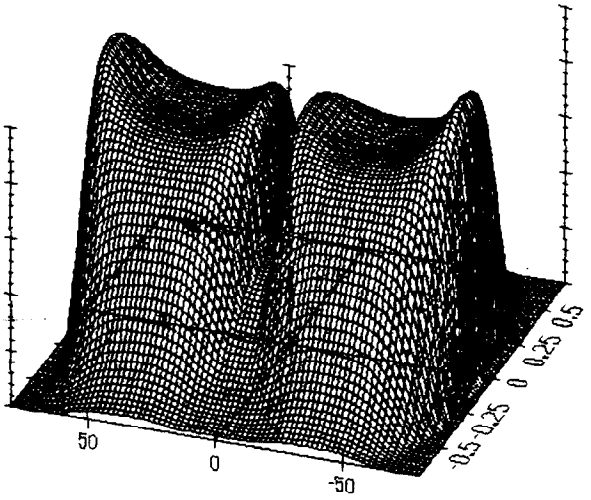

Fig. 6. The flux angular distribution.

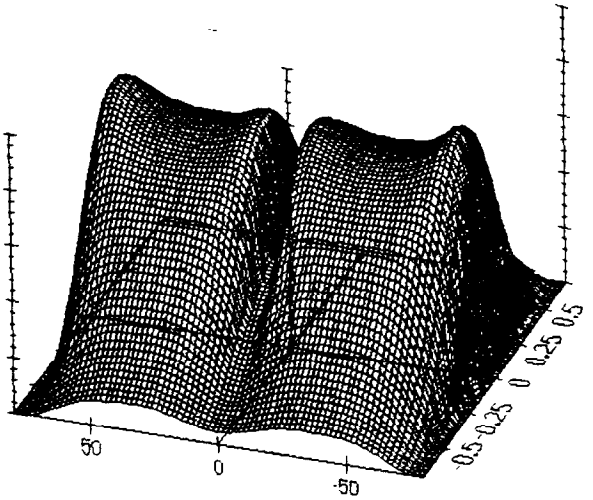

Fig. 7. The flux angular distribution.

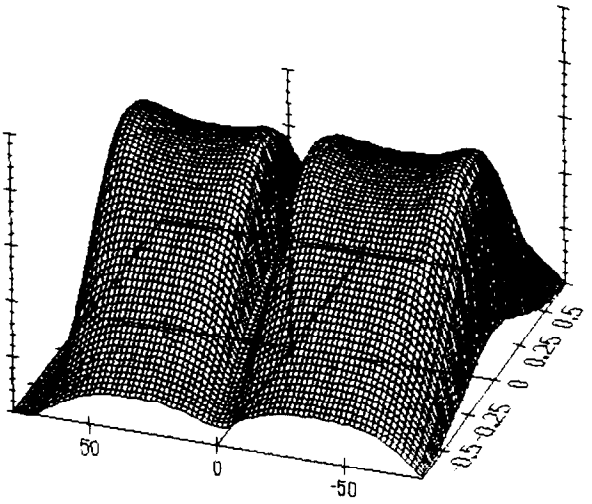

Fig. 8. The flux angular distribution.

parameters used are $\sigma_x = 2.6$ mm, $\sigma_{x'} = 0.58$ mrad, $\epsilon_x = 0.62$ mm mrad, $\sigma_y = 0.47$ mm, $\sigma_{y'} = 0.17$ mrad, $\epsilon_y = 0.048$ mm mrad. Electron energy $E_e = 1.6$ GeV, photon energy is at 1 keV if not mentioned explicitly.

Fig. 5 is the on-axis flux spectrum calculated under various conditions. The top curve is the zero emittance far field case with incoherent superposition of radiation from different points; the lower one is the emittance-included and far field case with coherent superposition; the bottom two curves are emittance-included and near field case, with coherent and incoherent superposition respectively. This picture shows the following features:

- The emittance effect is obvious, especially for high photon energy.
- The near field effect is obvious also, mainly due to enlargement of the emittance effect in this case.
- The radiation of the electron beam is really incoherent.

Figs. 6–8 show the flux angular distribution. Fig. 6 is the far field, emittance-excluded case; fig. 7 is the far field, emittance-included case and fig. 8 is the near field, emittance-included case. The horizontal distribution is much larger than the vertical distribution and strange-shaped because of the shape of $B_y(z)$.

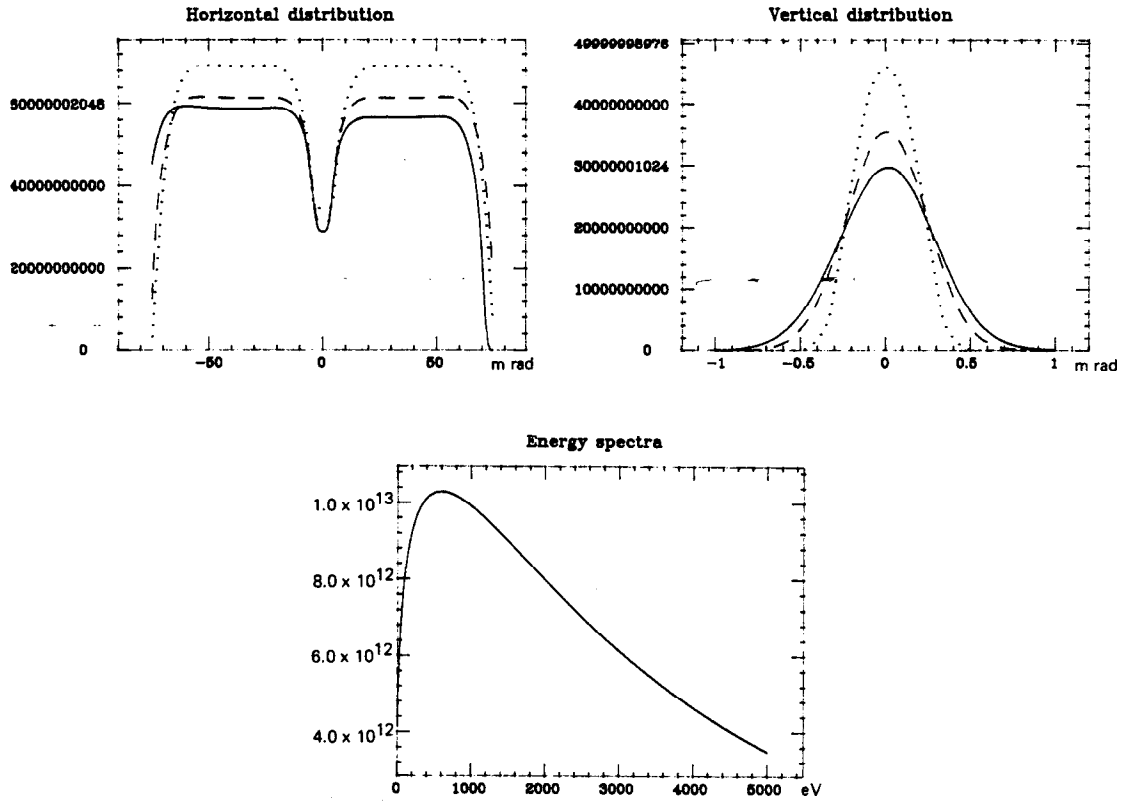

Fig. 9. The flux horizontal distribution.

Fig. 10. The flux vertical distribution.

Fig. 11. The spectra integrated over the solid angle.

The peak–valley structure of the horizontal distribution can be easily understood with the help of fig. 3. The influence of the near field and emittance are obvious although not very strong at this relatively low photon energy. The finite observation distance causes the horizontal distribution asymmetry and enlarges the emittance effect.

Fig. 9 is like figs. 6–8 but only the horizontal distribution is plotted and various cases are plotted in one picture for comparison. The vertical angle is at 0.3 mrad. The dotted curve is the far field zero emittance case; the dashed curve is the far field, emittance-included case; and the solid curve is the near field, emittance-included case.

Fig. 10 is similar to fig. 9 but the vertical distribution is plotted and the photon energy is 4 keV instead of 1 keV.

Fig. 11 shows the spectra integrated over the solid angle. Although there is only one curve, it actually consists of three sets of data, one is the far field zero emittance case, the others are near field cases with emittance excluded or included. The appearance of just one curve is demanded by the flux conservation law. So, this figure demonstrates that the output of RADID satisfies the flux conservation law, and supports our algorithm on dealing with near field and emittance.

5. Conclusion remark

The output of RADID is rich. The results are reasonable, especially for the consideration of emittance and observation distance; their effects are obvious, while the flux conservation law is satisfied. For an

undulator case, the algorithm may not be very accurate but be still good enough. To save space, no detailed discussion of RADID's output for undulators is given here.

Acknowledgement

We are grateful to the Insertion Device Group of the Synchrotron Radiation laboratory, BEPC, who provided us with the field distribution. Special thanks are due to Mrs. Jin Yalan, for her help on the computer-work and on the editing of this paper.

References

[1] Int. Conf. on Insertion Devices for Synchrotron Radiation Source, SPIE Proc. 582 (1985).
[2] J. Jackson, Classical Electrodynamics, 2nd ed. (Wiley, New York, 1975) chap. 14.
[3] C. Jacobsen and H. Rarback, SPIE 582 (1985) 201.
[4] H. Rarback et al., Nucl. Instr. and Meth. A266 (1988) 96.
[5] C. Leubner and H. Ritsch, Nucl. Instr. and Meth. A246 (1986) 45; and J. Phys. A19 (1986) 329.
[6] R.P. Walker, Nucl. Instr. and Meth. A267 (1988) 537.
[7] B. Kincaid, J. Opt. Soc. Am. B2 (1985) 1294; and Nucl. Instr. and Meth. A246 (1986) 109.
[8] S. Krinsky, M. Perlman and R. Watson, in: Handbook of Synchrotron Radiation, vol. 1A, ed. E. Koch (North-Holland, Amsterdam, 1983).
[9] E.S. Tang et al., Proc. Int. Conf. on Synchrotron Radiation Applications, Hefei, 1989, to be published.
[10] H. Winick, in: Applications of Synchrotron Radiation, ed. H. Winick, D. Xian, M.-H. Ye, T. Huang (Gordon and Breach, 1989).
[11] B. Lai and F. Cerrina, Nucl. Instr. and Meth. A246 (1986) 337.
[12] X-ray Data Booklet, ed. D. Vaughan (Center for X-Ray Optics, Lawrence Berkeley Lab., 1985).